Contemporary Mathematics

Conservative Front Tracking in One Space Dimension

James Glimm, Xiao Lin Li, and Yingjie Liu

Abstract. We propose a fully conservative Front Tracking algorithm in 1D and examine the close connection between the tracked front position error and the local truncation error near the front. The algorithm is second order accurate in L_1 for piecewise smooth solutions all of whose discontinuities are tracked, except for interactions of tracked waves. The local truncation errors in L_∞ are third order in the interior (away from tracked fronts) and away from local maxima, second order in L_∞ near isolated tracked fronts, and $\mathcal{O}(1)$ near the finite number of space time points at which tracked fronts collide. 1D Numerical tests confirming these theoretical estimates are presented.

1. Introduction

We propose and demonstrate a tracking finite difference algorithm which is (a) fully conservative and (b) improves local truncation error by one order (from $\mathcal{O}(1)$ to $\mathcal{O}(\Delta x)$ and to $\mathcal{O}(\Delta x^2)$ in 1D) near tracked discontinuities.

Discontinuities in the solutions of systems of nonlinear hyperbolic conservation laws are widely recognized as a primary difficulty for numerical simulation. Surprisingly, the nonlinearities actually help, as they cause information, which flows along solution characteristics, to flow into the discontinuity, and disappear there. The nonlinear discontinuities (shock waves) function much as a black hole in this regard. Included in this flow of information are the solution errors generated by the nonlinear discontinuity. Because the nonlinear discontinuities absorb errors associated with their numerical approximation, these errors do not grow or spread with time.

Nonlinear equations also have linear discontinuities. In gas dynamics these are the contact discontinuities, across which temperature or shear velocities can be discontinuous. Errors in these modes are never forgiven and never dissipated. For

2000 *Mathematics Subject Classification.* Primary 65M06; Secondary 65M12.

The first author was supported by the MICS program of the U.S. Department of Energy DE-FG02-90ER25084, Department of Energy Contract No. DE-AC02-98CH10886 and Office of Inertial Fusion, the Army Research Office, grant DAAD19-01-1-0642, the National Science Foundation, grant DMS-0102480 and Los Alamos National Lab Sponsor ID # 26730001014L.

The second author was supported by the U.S. Department of Energy, Sponsor ID # DEFG0398DP00206 and Los Alamos National Lab Sponsor ID # 26730001014L.

The third author was supported by the U.S. Department of Energy, Sponsor ID # DEFG0290ER25084 and Los Alamos National Lab Sponsor ID # 26730001014L.

this reason the linear modes are more difficult to control numerically. The dominant numerical solution error is typically associated with discontinuities in these linear modes and occurs as diffusion of mass, vorticity, and temperature. These errors increase with time.

Front Tracking was introduced to give special treatment to solution discontinuities. Perceptions that Front Tracking software difficulties would be insurmountable were too pessimistic, and a robust, validated code has been developed and used in production simulation of fluid instabilities [**6, 8, 7, 5**]. See also the URL http://www.ams.sunysb.edu/~shock/FTdoc/FTmain.html. Here we address an algorithmic issue: formulation of a conservative tracking algorithm. In its original formulation, conservation was enforced only in regular grid cells, those not cut by the tracked front. The missing points of the computation stencil, in the case of a front cutting through the stencil, are filled in as ghost cells, with the state values obtained by extrapolation from nearby front states of the same component. Thus the state values are double valued near the front, with the left-component states extending by extrapolation for a small distance into the right component, and *vice versa*. The use of ghost cell states was introduced into Front Tracking in 1980 [**10**]. With the ghost states thus defined, the interior solver follows a conventional finite difference algorithm.

In the level set method [**4**] and the original Front Tracking, ghost cells constructed near the front (but using entropy extrapolation) allows a standard difference operation update. As with Front Tracking, the ghost cell extrapolation is non conservative and leads to $\mathcal{O}(1)$ local truncation error.

Here we propose an algorithm which is conservative for all grid cells, including the irregular ones cut by the front. The algorithm we propose is related to earlier work of Swartz and Wendroff [**15**], Harten and Hyman [**12**], and Colella and Chern [**1**], but differs from these works in several ways. We emphasize here tracking of a contact, rather than the shock tracking of [**1**]. Our support for fronts is fully general and can be used for unstable, convoluted, and bifurcating interfaces. this algorithm is formally second order accurate in the L_1 norm except for interactions of tracked waves. More precisely, it has a third order local truncation error in the interior, away from tracked fronts and from local extrema, second order local truncation error near isolated tracked fronts and $\mathcal{O}(1)$ local truncation error near points of interaction of tracked waves. An important difference with [**15**] is our discussion of the extension to higher dimensions [**9**].

2. Conservative Tracking

Consider the one dimensional system of conservation laws

$$\frac{\partial u}{\partial t} + \frac{\partial f(u)}{\partial x} = 0 \ . \tag{1}$$

Weak or discontinuous solutions of this equation are not unique, and the equation must be supplemented by an entropy condition [**14**]. In the case of discontinuities, the partial derivatives in (1) are not defined, and Rankine-Hugoniot conditions

$$s[u] = [f] \tag{2}$$

apply. Here $[A]$ represents the jump $A_+ - A_-$ in the quantity A across the discontinuity, and $d\sigma/dt = s$ is the speed of the moving discontinuity $x = \sigma(t)$. In fact

(2) results from (1) if the partial derivatives in (1) are interpreted in the sense of distributions.

Let $\{x_i\}$ be the cell centers of a uniform partition of the spatial computational domain and let $\Delta x = x_{i+1} - x_i$. Integration of (1) over the rectangle $[x_{i-1/2}, x_{i+1/2}] \times [t_n, t_{n+1}]$ yields

$$U_j^{n+1} = U_j^n - \frac{\Delta t}{\Delta x}\left(F_{j+1/2}^{n+1/2} - F_{j-1/2}^{n+1/2}\right) , \tag{3}$$

where

$$U_j^n = \frac{1}{\Delta x}\int_{x_{j-1/2}}^{x_{j+1/2}} u(x, t_n)dx \tag{4}$$

represents the cell average of the solution $u(x,t)$ over the interval $[x_{j-1/2}, x_{j+1/2}]$, and

$$F_{j+1/2}^{n+1/2} = \frac{1}{\Delta t}\int_{t_n}^{t_{n+1}} f(u(x_{j+1/2}, t))dt \tag{5}$$

is the integral of the flux over a mesh time interval. Numerical approximations to the flux $F_{j+1/2}^{n+1/2}$ generate various conservative schemes [**13**] to approximate the weak solutions of the hyperbolic system (1). These schemes are conservative in the sense that the total conserved quantity of u in the computational domain is a constant whose value in time changes only due to the net influxes from the boundaries at each end of the domain. In general, let $\mathcal{U}_i^n$ be the approximation of U_i^n, and let $\mathcal{F}_{i+1/2}^{n+1/2}$ be the approximation of $F_{i+1/2}^{n+1/2}$. The numerical scheme can be written in the form

$$\mathcal{U}_j^{n+1} = \mathcal{U}_j^n - \frac{\Delta t}{\Delta x}\left(\mathcal{F}_{j+1/2}^{n+1/2} - \mathcal{F}_{j-1/2}^{n+1/2}\right) . \tag{6}$$

In this paper, we use the MUSCL scheme [**16, 17, 18, 3**] for simulations and for grid cell stencils in which no tracked interface occurs.

Traditional Front Tracking follows the same scheme in the interior region, which is defined as comprising those cells whose stencil does not intersect the tracked interface. However, Front Tracking uses the tracked interface to define interior boundaries. Ghost cells [**11**], which extrapolate the interface states, are used for the calculation of the flux for interior cell centers near the interface. This method is not conservative across the tracked interface if two different approximations of the flux on an edge between two cells are used. We consider an interface whose position at time t is $\sigma_e(t)$ and assume a linear approximation $\sigma(t)$ to $\sigma_e(t)$ on $[t_n, t_{n+1}]$.

The algorithm is divided into two cases. As a first case, we assume that the approximate interface does not cross a mesh cell center within the time interval $[t_n, t_{n+1}]$. Thus for some mesh index i, $x_i \le \sigma(t_n), \sigma(t_{n+1}) \le x_{i+1}$. We displace the cell boundary located at $x_{1+1/2}$ to the interface location. This change results in a redefinition of the cell average quantity (4), to yield

$$U_i^m = (\Delta_{i,e}^m)^{-1}\int_{x_{i-1/2}}^{\sigma_e(t_m)} u(x, t_m)dx , \tag{7}$$

$$U_{i+1}^m = (\Delta_{i+1,e}^m)^{-1}\int_{\sigma_e(t_m)}^{x_{i+3/2}} u(x, t_m)dx , \tag{8}$$

for $m = n, n+1$, where $\Delta_{j,e}^m$ is the interval over which U_j^m is averaged.

Denote by $\mathcal{U}_i^m$ on $[x_{i-1/2}, \sigma(t_m)]$ and $\mathcal{U}_{i+1}^m$ on $[\sigma(t_m), x_{i+3/2}]$ the numerical approximations of U_i^m and U_{i+1}^m respectively and let Δ_j^m be the interval over which $\mathcal{U}_j^m$ is averaged. Integrating the hyperbolic system over the two trapezoidal regions $[x_{i-1/2}, \sigma(t)] \times [t_n, t_{n+1}]$ and $[\sigma(t), x_{i+3/2}] \times [t_n, t_{n+1}]$, the finite difference equation (6) for irregular cells is replaced by

$$\Delta_i^{n+1} \mathcal{U}_i^{n+1} = \Delta_i^n \mathcal{U}_i^n - \Delta t \{ \mathcal{F}_{\text{int}}^{n+1/2} - \mathcal{F}_{i-1/2}^{n+1/2} \} , \tag{9}$$

$$\Delta_{i+1}^{n+1} \mathcal{U}_{i+1}^{n+1} = \Delta_{i+1}^n \mathcal{U}_{i+1}^n - \Delta t \{ \mathcal{F}_{i+3/2}^{n+1/2} - \mathcal{F}_{\text{int}}^{n+1/2} \} , \tag{10}$$

where $\mathcal{F}_{\text{int}}^{n+1/2}$ is the numerical approximation to the flux

$$F_{\text{int}}^{n+1/2} = \frac{1}{\Delta t} \int_{t_n}^{t_{n+1}} \left(f(u(\sigma_e(t), t)) - s_e u(\sigma_e(t), t) \right) dt \tag{11}$$

across the exact interface. Here $\sigma_e(t)$ and $s_e = d\sigma_e/dt$. The definition (11) gives equal values when evaluated on either side of the interface due to the Rankin-Hugoniot condition (2).

Let $s(t) = d\sigma/dt$ be the speed of the numerically tracked interface $\sigma(t)$. The choice of the numerical shock speed is discussed in [**2**]. Assume a smooth solution in the interior region excluding the tracked waves. Also we assume that the Riemann solution associated with (1) depends Lipschitz-continuously on the left and right states which define the Riemann problem. Using a 2nd order MUSCL reconstruction, we first reconstruct a piecewise linear function on each cell out of the cell averages at $t = t_n$ to yield the approximate left and right states $\mathcal{U}_l^n, \mathcal{U}_r^n$ at $\sigma_e(t_n)$, so that $\mathcal{U}_l^n - u(\sigma_e(t_n)-, t_n) = \mathcal{O}(\Delta x^2)$ and $\mathcal{U}_r^n - u(\sigma_e(t_n)+, t_n) = \mathcal{O}(\Delta x^2)$. Solving the Riemann problem with the above two approximate states we obtain a shock speed s^n which satisfies $s^n - s_e(t_n) = \mathcal{O}(\Delta x^2)$. Therefore the approximate tracked interface position at $t = t_n + \frac{1}{2}\Delta t$ is

$$\sigma^{n+1/2} = \sigma(t_n) + \frac{1}{2}\Delta t \cdot s^n = \sigma_e(t_{n+1/2}) + \mathcal{O}(\Delta t^2) .$$

Using a Taylor expansion we reconstruct the approximate left and right states $\mathcal{U}_l^{n+1/2}, \mathcal{U}_r^{n+1/2}$ at $(\sigma^{n+1/2}, t_{n+1/2})$ from the MUSCL reconstruction, so that

$$\mathcal{U}_l^{n+1/2} - u(\sigma_e(t_{n+1/2})-, t_{n+1/2}) = \mathcal{O}(\Delta x^2), \tag{12}$$

and

$$\mathcal{U}_r^{n+1/2} - u(\sigma_e(t_{n+1/2})+, t_{n+1/2}) = \mathcal{O}(\Delta x^2). \tag{13}$$

Finally, solving a Riemann problem with the left and right states $\mathcal{U}_l^{n+1/2}$ and $\mathcal{U}_r^{n+1/2}$ we obtain the half time step shock speed $s^{n+1/2} = s_e(t_{n+1/2}) + \mathcal{O}(\Delta t^2)$, and the new two sides states $\mathcal{U}_{l1}^{n+1/2}$ and $\mathcal{U}_{r1}^{n+1/2}$ across the interface we want to track. Since the exact solution is smooth near the interface, the new states still satisfy (12) and (13).

This construction gives a local truncation error $\mathcal{O}(\Delta x^3)$ for the propagated shock position

$$\sigma_e^{n+1} = \sigma^n + s^{n+1/2}\Delta t + \mathcal{O}(\Delta t^3) .$$

In fact,

$$
\begin{aligned}
\sigma_e^{n+1} - \sigma^n &= \int_{t_n}^{t_{n+1}} s_e(t)dt \\
&= \int_{t_n}^{t_{n+1}} [s_e(t_{n+1/2}) + s_e'(t_{n+1/2})(t - t_{n+1/2}) + \mathcal{O}(\Delta t^2)]dt \qquad (14)\\
&= s_e(t_{n+1/2})\Delta t + \mathcal{O}(\Delta t^3) \ .
\end{aligned}
$$

to give the desired accuracy. Let the numerical flux across the tracked front associated with the Riemann problem defined by these two states be

$$\mathcal{F}_i^{n+1/2} = f(\mathcal{U}_{l1}^{n+1/2}, t_{n+1/2}) - s^{n+1/2}\mathcal{U}_{l1}^{n+1/2}.$$

This flux satisfies

$$\mathcal{F}_i^{n+1/2} = F_i^{n+1/2} + \mathcal{O}(\Delta x^2)$$

and is continuous when evaluated from either side of the discontinuity.

Since the width of each trapezoidal region is greater than $\Delta x/2$, we can choose the CFL coefficient to be $1/2$.

As the second case of the algorithm, we suppose that the front crosses a mesh cell center. Due to a CFL restriction on the time step it can cross at most one mesh cell center in the time interval $[t_n, t_{n+1}]$. Thus we can assume $x_i \le \sigma(t_n) \le x_{i+1}$ for some mesh index i, and either (a) $x_{i-1} < \sigma(t_{n+1}) < x_i$ or (b) $x_{i+1} < \sigma(t_{n+1}) < x_{i+2}$. We only discuss case (b), since case (a) is similar. It is convenient to remove the cell (with cell average $\mathcal{U}_{i+1}$), and combine each of its two fractional pieces with the neighbor cell on the corresponding side of the interface. Thus we retain (7) for $m = n$ and (8) for $m = n+1$ with i replaced by $i+1$, but we also require averages over enlarged cells with fractional pieces added to a full cell. This requirement leads to the definitions

$$\overline{U}_i^{n+1} = (\overline{\Delta}_{i,e}^{n+1})^{-1} \int_{x_{i-1/2}}^{\sigma_e(t_{n+1})} u(x, t_{n+1})dx \ ,$$

$$\overline{U}_{i+2}^{n} = (\overline{\Delta}_{i+2,e}^{n})^{-1} \int_{\sigma_e(t_n)}^{x_{j+5/2}} u(x, t_n)dx \ ,$$

where $\overline{\Delta}_{j,e}^m$ denotes the length of the averaging interval in the above integrals. Denote by $\overline{\mathcal{U}}_i^{n+1}$ on $[x_{i-1/2}, \sigma(t_{n+1})]$ and $\overline{\mathcal{U}}_{i+2}^n$ on $[\sigma(t_n), x_{i+5/2}]$ the numerical approximation to $\overline{U}_i^{n+1}$ and $\overline{U}_{i+2}^n$ respectively. Let $\overline{\Delta}_j^m$ denote the averaging interval for $\overline{\mathcal{U}}_j^m$.

Integrating the hyperbolic system over the two trapezoidal regions $[x_{i-1/2}, \sigma(t)] \times [t_n, t_{n+1}]$ and $[\sigma(t), x_{i+5/2}] \times [t_n, t_{n+1}]$, we require

$$\overline{\Delta}_i^{n+1}\overline{\mathcal{U}}_i^{n+1} = \Delta_i^n\mathcal{U}_i^n - \Delta t\{\mathcal{F}_{\text{int}}^{n+1/2} - \mathcal{F}_{i-1/2}^{n+1/2}\} \ , \tag{15}$$

$$\Delta_{i+2}^{n+1}\mathcal{U}_{i+2}^{n+1} = \overline{\Delta}_{i+2}^{n+1}\overline{\mathcal{U}}_{i+2}^n - \Delta t\{\mathcal{F}_{i+5/2}^{n+1/2} - \mathcal{F}_{\text{int}}^{n+1/2}\} \ , \tag{16}$$

with the flux $\mathcal{F}_{\text{int}}^{n+1/2}$ constructed as above. We assume, as a condition on the prior time step,

$$\overline{\Delta}_{i+2}^n\overline{\mathcal{U}}_{i+2}^n = \Delta_{i+1}^n\mathcal{U}_{i+1}^n + \Delta x\, \mathcal{U}_{i+2}^n \ .$$

For the reconstruction of $\mathcal{U}_i^{n+1}$ and $\mathcal{U}_{i+1}^{n+1}$ from $\overline{\mathcal{U}}_i^{n+1}$, we require

$$\overline{\Delta}_i^{n+1}\overline{\mathcal{U}}_i^{n+1} = \Delta x\mathcal{U}_i^{n+1} + \Delta_{i+1}^{n+1}\mathcal{U}_{i+1}^{n+1} \ . \tag{17}$$

To complete the definition of the algorithm in the second case, we approximate the slope of u at the cell center $\frac{1}{2}(x_{i-1/2}+\sigma(t_{n+1}))$ by the first order, say slope_0. A limiter

$$\text{slope}_0 = \text{minmod}\{\text{slope}_1, \text{slope}_2\}, \tag{18}$$

accomplishes this approximation, where

$$\begin{array}{lcl} \text{slope}_1 & = & (\mathcal{U}_{i-1}^{n+1} - \mathcal{U}_{i-2}^{n+1})/\Delta x \ , \\ \text{slope}_2 & = & (\overline{\mathcal{U}}_i^{n+1} - \mathcal{U}_{i-1}^{n+1})/(\frac{\sigma(t_{n+1})-x_{i-3/2}}{2}) \ , \\ \text{minmod}\{a,b\} & = & 0 \text{ if } ab \leq 0; \ \text{sgn}(a)\min\{|a|,|b|\} \text{ otherwise.} \end{array} \tag{19}$$

Let $L(x) = \overline{\mathcal{U}}_i^{n+1} + \text{slope}_0 * (x - (\sigma(t_{n+1}) + x_{i-1/2})/2)$. We assign $\mathcal{U}_i^{n+1}$ and $\mathcal{U}_{i+1}^{n+1}$ to be the values of $L(x)$ at their corresponding cell centers. We have

$$\begin{array}{lcl} \mathcal{U}_i^{n+1} & = & \overline{\mathcal{U}}_i^{n+1} + \text{slope}_0 \cdot (x_i - \frac{x_{i-1/2}+\sigma(t_{n+1})}{2}) \ , \\ \mathcal{U}_{i+1}^{n+1} & = & \overline{\mathcal{U}}_i^{n+1} + \text{slope}_0 \cdot (\frac{x_{i+1/2}+\sigma(t_{n+1})}{2} - \frac{x_{i-1/2}+\sigma(t_{n+1})}{2}) \ . \end{array} \tag{20}$$

A simple calculation verifies (17). Then the quantity

$$S^n = \sum_j \Delta_j^n \mathcal{U}_j^n \tag{21}$$

is conserved.

PROPOSITION 1. *The algorithm defined by (3), (9) - (17) is conservative in the sense that the quantity S^n of (21) is preserved from time step to time step, up to modification by flux through the boundary of the domain.*

PROOF. The conservation of (21) is due to the cancelation of the flux terms in the time increment of (21), as defined by the difference equation for regular and irregular cells. The flux terms cancel because they have identical definitions for either side of a regular cell or moving interface to define an irregular cell boundary. At a continuum level the Rankine-Hugoniot relations guarantee that the integrand of (11) is single valued when evaluated along the interface, even though the individual terms are discontinuous there. We achieve this property in the finite difference scheme by choice of $\mathcal{F}_i^{n+1/2}$.

Consider next the case of nearby interfaces, for which a stencil is doubly irregular, in that the stencil cells overlap with the neighboring interface as well as with the interface of the stencil itself. By degrading the order of accuracy, we can shrink the stencil size and preserve the conservative nature of the algorithm. But eventually, the two interfaces are too close to accommodate a reduced size stencil. At this time the two interfaces are merged prematurely. The merger is accomplished by eliminating tracking for one of the tracked waves. Thus premature merging of fronts, or fronts with overlapping stencils is a special case of fronts which will no longer be tracked. To eliminate tracking while preserving conservation, it is necessary to redistribute the material in the two irregular cells on each side of the front into the two or three cells which these irregular cells occupy. Redistribution of material is accomplished by volume weighted average to determine the total material in the union of these cells and an equal division to divide the total material among the two or three regular cells.

Thus the proof of conservation remains valid for cases where tracking is terminated, including the case of wave interactions. $\square$

PROPOSITION 2. *The reconstruction near the interface, together with (6), (9) and (10) defines a conservative finite difference scheme which is formally second order accurate in the L_1 norm for piecewise smooth solutions all of whose discontinuities are tracked, except for the interactions of tracked waves. Specifically, the L_∞ truncation errors are third order away from the tracked fronts and from local extrema, second order near isolated tracked fronts and local extrema, and $\mathcal{O}(1)$ near intersecting tracked fronts.*

PROOF. We obtain three separate bounds on the L_∞ local truncation error. For regular grid states, whose stencil does not meet the tracked front, the L_∞ local truncation error is $\mathcal{O}(\Delta x^3)$. This estimate is a standard property of MUSCL and is not repeated here. For singly irregular cells, whose stencil meets exactly one tracked front, we derive the bound $\mathcal{O}(\Delta x^2)$ on the L_∞ local truncation error. For multiply irregular cells, whose stencil meets two or more tracked waves, we have the trivial $\mathcal{O}(1)$ L_∞ local truncation error bound. The first two types of errors contribute $\mathcal{O}(\Delta x^3)$ to the global L_1 error for a single time step and thus formally they contribute $\mathcal{O}(\Delta x^2)$ to the global L_1 error bound after integration to a fixed physical time T.

We next prove accuracy for the singly irregular cells. We solve (1) starting from time t_n. Then $\mathcal{U}^n = U^n$ are the averages of the initial solution over the corresponding cells, and $\sigma(t_n) = \sigma_e(t_n)$. We have already established the bounds

$$\begin{array}{rcl} \sigma(t_{n+1}) & = & \sigma_e(t_{n+1}) + \mathcal{O}(\Delta x^3) \ , \\ \mathcal{F}_{\mathrm{int}}^{n+1/2} & = & F_{\mathrm{int}}^{n+1/2} + \mathcal{O}(\Delta x^2) \ . \end{array} \tag{22}$$

The flux $\mathcal{F}_{i+1/2}^{n+1/2}$ is computed as in the MUSCL scheme [**3**] and satisfies

$$\mathcal{F}_{i-1/2}^{n+1/2} = F_{i-1/2}^{n+1/2} + \mathcal{O}(\Delta x^2) \ . \tag{23}$$

In the first case for the algorithm, we compare (9) with the equation satisfied by the exact solution and conclude that

$$\Delta_i^{n+1}\mathcal{U}_i^{n+1} - \Delta_{i,e}^{n+1}U_i^{n+1} = \mathcal{O}(\Delta x^3) \ , \tag{24}$$

which gives the required local truncation error near the interface

$$\begin{array}{rcl} \mathcal{U}_i^{n+1} - U_i^{n+1} & = & (\Delta_{i,e}^{n+1}/\Delta_i^{n+1})U_i^{n+1} - U_i^{n+1} + \mathcal{O}(\Delta x^2) \\ & = & \mathcal{O}(\Delta x^2) \ . \end{array} \tag{25}$$

We next suppose that we are in the second case of the algorithm. An argument similar to that of (24), (25) leads to $\overline{\mathcal{U}}_i^{n+1} - \overline{U}_i^{n+1} = \mathcal{O}(\Delta x^2)$. Because of this bound and because the exact solution is smooth on each side of the tracked interface, we have $\mathrm{slope}_1 = \mathrm{slope}_2 + \mathcal{O}(\Delta x) = \mathrm{slope}_0 + \mathcal{O}(\Delta x)$. With the help of $\sigma(t_{n+1}) - \sigma_e(t_{n+1}) = \mathcal{O}(\Delta x^3)$ we have $u(\frac{x_{i-1/2}+\sigma(t_{n+1})}{2}, t_{n+1}) - \overline{U}_i^{n+1} = \mathcal{O}(\Delta x^2)$. Therefore $\frac{\partial u}{\partial x}(\frac{x_{i-1/2}+\sigma(t_{n+1})}{2}, t_{n+1}) - \mathrm{slope}_0 = \mathcal{O}(\Delta x)$. We obtain

$$\begin{array}{rcl} \mathcal{U}_i^{n+1} & = & u(x_i, t_{n+1}) + \mathcal{O}(\Delta x^2) \\ & = & U_i^{n+1} + \mathcal{O}(\Delta x^2), \\ \mathcal{U}_{i+1}^{n+1} & = & u((x_{i+1/2} + \sigma(t_{n+1}))/2, t_{n+1}) + \mathcal{O}(\Delta x^2) \\ & = & U_{i+1}^{n+1} + \mathcal{O}(\Delta x^2) \ , \end{array} \tag{26}$$

which establishes second order accuracy in the second case.

If $\mathcal{U}$,U fall into logically different cases, *i.e.*, if the exact and approximate shocks at time level $t = t_{n+1}$ are on different sides of a mesh cell center, then the definitions

Method	N	L_1 error	L_1 order	$\Sigma U_i \Delta x_i$
Un-tracked	30	6.83e-2	-	1.732
	60	3.49e-2	0.969	1.733
	120	1.63e-2	1.10	1.733
	240	8.24e-3	0.984	1.733
Non-conservatively tracked	30	2.80e-2	-	1.721
	60	6.89e-3	2.02	1.716
	120	4.23e-3	0.704	1.742
	240	2.01e-3	1.07	1.741
Conservatively tracked	30	2.17e-2	-	1.732
	60	7.07e-3	1.62	1.733
	120	2.11e-3	1.74	1.733
	240	6.04e-4	1.80	1.733

TABLE 1. Comparative error analysis for the test problem (27) for Burgers' equation.

of $\mathcal{U}_i^{n+1}$ and U_i^{n+1} are not the same. In this case, the shock position must be within $\mathcal{O}(\Delta x^3)$ of lying exactly at a cell center, a case which allows treatment as a regular cell. Thus in this case the two logically different cases are, within our error bounds, both treatable as regular cells, and thus both treatable as falling in the same logical case. □

3. Numerical Examples

Consider the Burgers' equation $\frac{\partial u}{\partial t} + \frac{\partial}{\partial x}(\frac{1}{2}u^2) = 0$ on $[0, 6] \times [0, T]$, with initial conditions

$$u(x, 0) = \begin{cases} 0.2 * (x-1)^2 + 0.2\ , & x \in [1, 3]\ , \\ 0.2\ , & \text{elsewhere}\ . \end{cases} \tag{27}$$

In Table 1 we present the numerical results at $T = 3.2$ using three different methods: the untracked MUSCL scheme, non-conservatively (shock) tracked scheme with MUSCL interior solver and conservatively (shock) tracked scheme with MUSCL interior solver. Fig. 1 displaces the comparative numerical results obtained with $N = 30$, $T = 3.2$ and CFL number equal to 0.4. Here L_1 error indicates the L_1 norm of $u - \tilde{U}$ at time T, where u is the exact solution and $\tilde{U}$ is the 2nd order approximate solution reconstructed from the piecewise constant numerical solution U at time T, which is supposed to be an approximation of the cell average of the the exact solution. Next we study a shock contact interaction problem for the Euler equation for one dimensional ideal gas, with $\gamma = 1.4$. For the conservative and non-conservative front tracking methods, only the contact discontinuities are tracked. The computational domain is $[0, 4]$ with flow-through boundary conditions. The initial states are given as follows. The density, pressure, and velocity are $2, 0.5, 0$ on $[0, 1]$; $0.5, 0.5, 0$ on $(1, 2)$; and $0.4, 4, -1$ on $[2, 4]$. The density and pressure plots at different time levels are shown from Fig. 2 to Fig. 5. In Table 2 we compare the total conservative quantities for the three methods. The test problem is made up of two Sod problems so that we have periodic boundary conditions. Hence the net influx is zero during the time evolution. The density, pressure, and velocity are $1, 1, 0$ on $[0, 2]$; $0.125, 0.1, 0$ on $(2, 4)$; and $1, 1, 0$ on $[4, 6]$. We only track the contact

Method	T	mass	momentum	total energy
Untracked or Conservatively tracked	0.32	4.250000	0.000000	10.50000
	0.67	4.250000	0.000000	10.50000
	0.82	4.250000	0.000000	10.50000
	1.00	4.250000	0.000000	10.50000
Non-conservatively tracked	0.32	4.250281	-0.000542	10.49988
	0.67	4.249588	0.000101	10.49958
	0.82	4.256037	0.00270	10.51241
	1.00	4.249498	0.00447	10.50836

TABLE 2. Comparative total conservative quantities for a shock contact interaction in gas dynamics

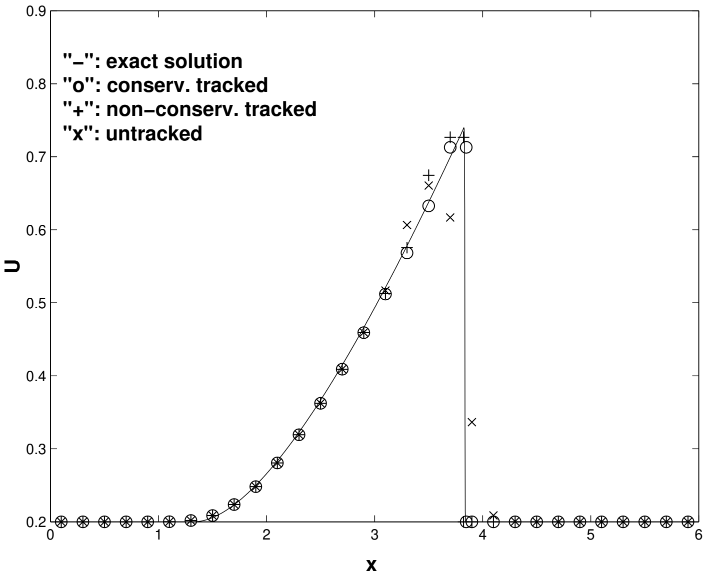

FIGURE 1. Comparative numerical results for Burgers' equation

discontinuity bifurcated from the Riemann problem at $x = 4$ for the two tested tracking methods. The computational domain $[0, 6]$ is partitioned evenly into 300 cells. The total mass, momentum and energy in the computational domain for the two conserved methods show essentially perfect agreement, while the non conserved tracking shows conservation errors in the third or fourth digit. In particular, the error in momentum increases when the shocks start to interact with the tracked contact around and after time $t = 0.82$.

4. Conclusions

We have proposed a conservative front tracking scheme with improved accuracy. It is in addition fully second order accurate away from intersection of tracked waves. Extension of the algorithm to 2D is developed in [**9**], based on a space

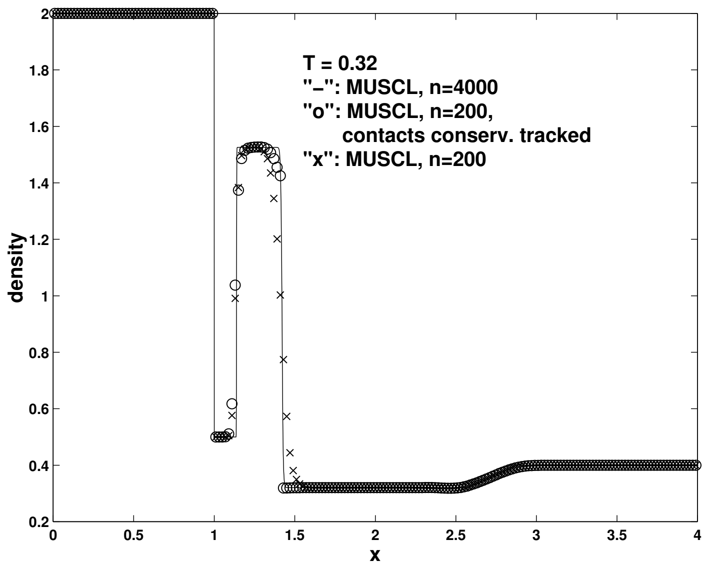

FIGURE 2. A left facing shock at $x = 1.2$ from a Riemann problem is about to interact with a contact at $x = 1$. Shown here: density *vs* distance.

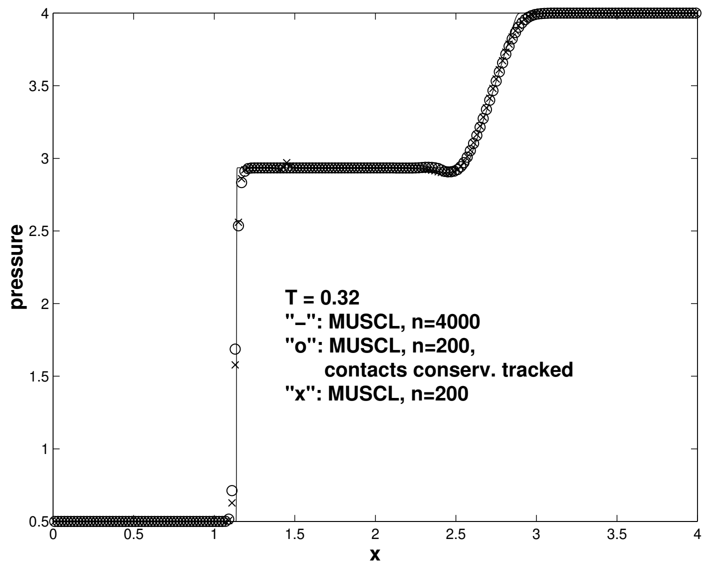

FIGURE 3. Pressure *vs* distance for the same simulation as in Fig. 2.

time tracked interface. Numerical tests in 1D demonstrate the properties of the algorithm. For the problem of Table 1, we note that non conservatively tracked algorithm improves significantly over the untracked scheme for coarse grids, but loses much of its advantage for very fine grids. The conservatively tracked scheme shows

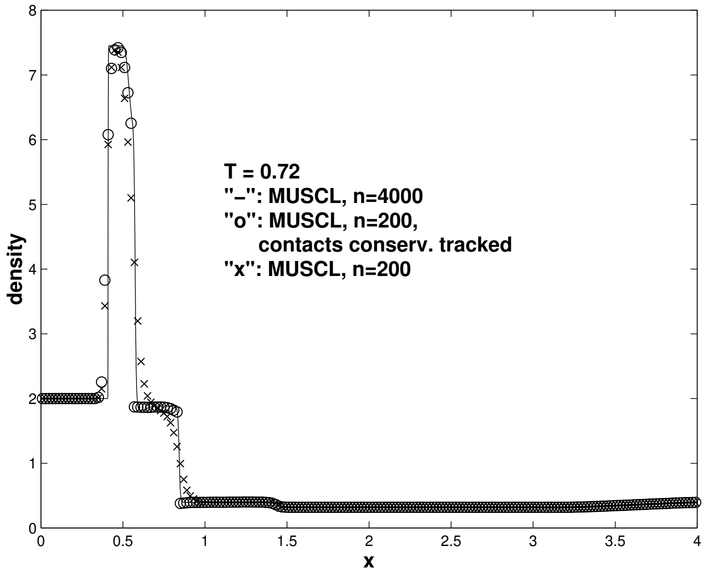

FIGURE 4. Density *vs* distance plot for the problem of Fig. 2 after the left facing shock has interacted with the large contact.

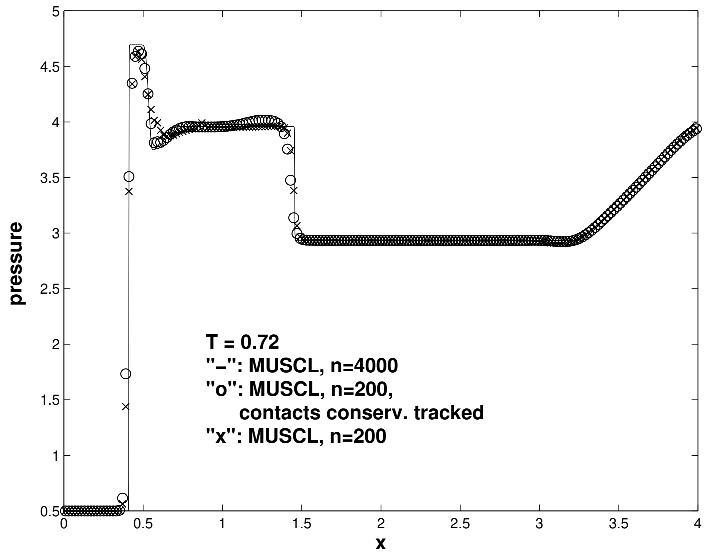

FIGURE 5. Pressure *vs* distance plot for the problem of Fig. 4.

near second order accuracy for all levels of grid refinement for Burgers' equation, and improves its accuracy relative to the untracked solution as the grid is refined.

For applications to gas dynamics in higher dimensions we did not track the shocks, which is why they are untracked in the 1D gas dynamics example. We note the significant improvement in the conservation properties for the new scheme.

References

[1] I-L. Chern and P. Colella. A conservative front tracking method for hyperbolic conservation laws. LLNL Rep. No. UCRL-97200, Lawrence Livermore National Laboratory, 1987.

[2] I-L. Chern, J. Glimm, O. McBryan, B. Plohr, and S. Yaniv. Front tracking for gas dynamics. *J. Comput. Phys.*, 62:83–110, 1986.

[3] P. Colella. A direct Eulerian MUSCL scheme for gas dynamics. *SIAM Journal on Computing*, 6(1):104–117, 1985.

[4] R. P. Fedkiw, T. Aslam, B. Merriman, and S. Osher. A non-oscillatory Eulerian approach to interfaces in multimaterial flows (the ghost fluid method). *J. Comp. Phys.*, 152:457–492, 1999.

[5] J. Glimm, J. W. Grove, X. L. Li, W. Oh, and D. H. Sharp. A critical analysis of Rayleigh-Taylor growth rates. *J. Comp. Phys.*, 169:652–677, 2001.

[6] J. Glimm, J. W. Grove, X.-L. Li, K.-M. Shyue, Q. Zhang, and Y. Zeng. Three dimensional front tracking. *SIAM J. Sci. Comp.*, 19:703–727, 1998.

[7] J. Glimm, J. W. Grove, X.-L. Li, and D. C. Tan. Robust computational algorithms for dynamic interface tracking in three dimensions. *SIAM J. Sci. Comp.*, 21:2240–2256, 2000.

[8] J. Glimm, J. W. Grove, X.-L. Li, and N. Zhao. Simple front tracking. In G.-Q. Chen and E. DiBebedetto, editors, *Contemporary Mathematics*, volume 238, pages 133–149. Amer. Math. Soc., Providence, RI, 1999.

[9] J. Glimm, X.-L. Li, and Y.-J. Liu. Conservative front tracking in higher space dimensions. *Proceedings of International Workshop on Computational Methods for Continuum Physics and Their Applications (IWCCPA). In Press*, 2001. Report SUNYSB-AMS-01-17.

[10] J. Glimm, D. Marchesin, and O. McBryan. Subgrid resolution of fluid discontinuities II. *J. Comput. Phys.*, 37:336–354, 1980.

[11] J. Glimm, D. Marchesin, and O. McBryan. A numerical method for two phase flow with an unstable interface. *J. Comput. Phys.*, 39:179–200, 1981.

[12] A. Harten. High resolution scheme for hyperbolic conservation laws. *J. Comp. Phys.*, 49:357, 1983.

[13] R. LeVeque. *Numerical Methods for Conservation Laws.* Birkhäuser Verlag, Basel–Boston–Berlin, 1992.

[14] J. Smoller. *Shock Waves and Reaction-Diffusion Equations.* Springer-Verlag, New York, second edition, 1994.

[15] B. Swartz and B. Wendroff. Aztec: A front tracking code based on Godunov's method. *Appl. Num. Math.*, 2:385–397, 1986.

[16] B. van Leer. Toward the ultimate conservative difference scheme: II. monotonicity and conservation combined in a second order scheme. *J. Comput. Phys.*, 14:361–370, 1974.

[17] B. van Leer. Toward the ultimate conservative difference scheme: III. upstream-centered finite-difference schemes for ideal compressible flow. *J. Comput. Phys.*, 23:263–275, 1977.

[18] B. van Leer. Towards the ultimate conservative difference scheme: V. A second order sequel to Godunov's method. *J. Comput. Phys.*, 32:101–136, 1979.

Department of Applied Mathematics and Statistics, SUNY at Stony Brook, NY 11794-3600

Center for Data Intensive Computing, Brookhaven National Laboratory, Upton, NY 11793-5000

E-mail address: `glimm@ams.sunysb.edu`

Department of Applied Mathematics and Statistics, SUNY at Stony Brook, NY 11794-3600

E-mail address: `linli@ams.sunysb.edu`

Department of Applied Mathematics and Statistics, SUNY at Stony Brook, NY 11794-3600

E-mail address: `yingjie@ams.sunysb.edu`